2023 62nd IEEE Conference on Decision and Control (CDC)
December 13-15, 2023. Marina Bay Sands, Singapore

# On roll stabilisation using a canting keel

Hossein Ramezani[1], Shouvik Chaudhuri[1], Jerome Jouffroy[1], Arnd Baurichter[2], and Steen Mattrup Hansen[2]

***Abstract*— This paper presents a study on the modeling and control of a roll stabilization mechanism based on a canting keel. Compared to several active anti-rolling systems, it has the advantage of working at zero and non-zero surge velocity, while taking minimal space in the hull of a considered ship. Using first principles, we describe a simple nonlinear model of the system representing the roll motion of a ship equipped with a canting keel system. We then consider a few dynamic properties of the system under consideration, including the non-minimum phase behavior occurring when the keel is positively buoyant, dubbed as "Airkeel". A controller is then proposed to stabilize the roll motion to compensate for load unbalance of the ship and decrease the influence of waves. A few simulations results are presented for illustration.**

## I. Introduction

In marine environments, crew and passengers aboard a vessel, often encounter seasickness, characterized by the symptoms of dizziness, nausea and vomiting [1]. The major factors which cause such a form of motion sickness arise from the amplitude and frequency of vertical accelerations induced by roll motions of the vessel, particularly at locations away from the central line of the vessel. This reduces human comfort and affects their performance on the vessel [2]–[4].

Numerous anti-rolling mechanisms have been proposed over the last century [5], and can be classified as being either passive or active. Passive mechanisms are designed to provide damping of roll motion by increasing the ship's resistance to roll and commonly include bilge keels, stabilizer fins, and anti-heeling tanks [6]–[10]. Active anti-rolling systems are designed to control the roll motion of the ship via an actuating element and commonly include gyroscopic stabilizers, active fin stabilizers, rudder-roll stabilization systems etc. [11]–[15]. Gyroscopic stabilizers are highly effective in most sea states, and do not increase drag or reduce speed, work at zero surge velocity, but are quite heavy and can take significant space on the bridge of a ship. Active fin stabilizers are particularly effective in moderate to rough seas, and do not increase drag or reduce speed as well. Finally, rudder roll stabilization systems have the primary advantage of an enhancement in stability which results in less drag, thereby reducing fuel consumption and increasing overall speed.

[1] Hossein Ramezani, Shouvik Chaudhuri, and Jerome Jouffroy are with Centre for Industrial Mechanics (CIM), Department of Mechanical and Electrical Engineering (DME), University of Southern Denmark (SDU), Sønderborg, Denmark ramezani@sdu.dk; chaudhuri@sdu.dk; jerome@sdu.dk

[2] Arnd Baurichter and Steen Mattrup Hansen are with Dacoma ApS, Svendborg, Denmark ab@dacoma-dk.com; smh@dacoma-dk.com


Fig. 1. Photographic view of the ProZero Demo boat equipped with the novel *Airkeel* mechanism (Courtesy: Dacoma ApS and ProZero, Tuco Marine Group)

A canting keel is a system commonly found in high-performance racing sailboats such as the Volvo Ocean Racer, which is used to increase stability and speed. Similarly to a conventional keel, it is a form of ballast system and is typically made up of a heavy weight, such as lead or steel, suspended from an arm. However, in the case of a canting keel, the arm is attached to the hull or keel of the vessel via a hinge or other mechanism that allows it to be swung laterally. This movement is controlled by a hydraulic or electric drive that adjusts the angle of the ballast, thus providing restoring moments to the vessel. The swinging ballast system is used on racing sailboats to counteract the force of wind on the sails and keep the boat upright. However, it can also be useful on larger cruising boats as well, providing added stability in rough seas. This can help to keep the vessel safe in challenging conditions, improving safety for crew and passengers, while also giving the potential to compensate for load unbalance created by a crane on the ship, for example. As a further improvement on conventional canting keels, whose ballast is made up of lead or steel, the development of an air-filled canting keel, known as the *Airkeel* by Dacoma ApS is noteworthy (see figure 1). It reduces the overall weight of the system, making it possible to increase the cargo and crane capacity up to a factor of two [16]. This technology can be applied for a range of vessels including work and crew boats, crew transfer vessels, leisure boats, and super yachts [16]. The airkeel may also be a viable alternative to fin stabilizers since it provides roll damping at zero surge speed.

This paper investigates modeling and control of a canting keel mechanism for roll stabilization of a monohull marine vessel, described by a model developed from first principles

and utilized for diverse operations in the marine world. In order to tackle the model uncertainties and parametric variations arising from various sources, a sliding mode controller is chosen. It should be noted here that the objective is to achieve stability of the zero dynamics of the system under investigation, thereby driving the vessel to acceptable roll bounds under both matched and unmatched perturbations. This is known to be a challenge since the presence of transmission zeros may lead to non-minimum phase (NMP) behaviours of the system, which in turn impose some limitations on tracking as shown in [17], thereby affecting the system performance. A similar control design approach has been investigated earlier by [18], based on the works of [17], for rudder-roll damping system and course keeping of ships. The possibility of reduction in roll acceleration is also examined since it may lead to seasickness reduction as well.

The rest of the paper is organized as follows. In Section II, the mathematical model of the ship roll dynamics and the servo motor driving the keel mechanism are described. In Section III, the dynamical properties of such vessels, equipped with keel mechanisms are explained. In Section IV, the control design for such a system exhibiting non-minimum phase behaviour considering matched and unmatched disturbances using sliding mode are presented. In Section V, the potential of our approach is demonstrated with the help of case studies involving roll damping from an initial angle, unbalanced loading scenario and wave-induced disturbances. The controller performance is further analysed with a couple of performance metrics. Brief concluding remarks end this paper.

## II. Mathematical Model

In this section, the keel-equipped marine vessel along with the torque components acting upon the vessel are modelled based on the lumped parameter approach dependent on first principles, typical in the marine control community [3], [19]. The servo motor driving the keel mechanism has also been modelled separately.

### A. Model of marine vessel equipped with a keel mechanism

A monohull marine vessel equipped with a *keel* mechanism from a hinge point at the bottom of the hull and driven by a motor is considered for the purpose of modelling. The primary assumptions made during the development of the model are as follows:

- *Rigid Bodies*: Hull and the keel are assumed to be rigid bodies. No bending or torsion is considered.
- *Negligible Coupling*: The coupling between roll and yaw is assumed to be negligible. A 1-DoF model [4], [12] has been considered.

Based on these assumptions, the nonlinear roll-dynamics model for the keel-equipped marine vessel as shown in Fig. 2, can be represented by a lumped parameter model, which can be written as [3], [20],

$$\begin{aligned}(I_x + \Delta I_x)\dot{p} + K_p p + K_{p|p|} p|p| + \rho g \nabla \overline{GM}_m \phi \\ + K_{\phi^3}\phi^3 = \tau_k + \tau_d + \tau_{wi}\end{aligned} \tag{1}$$

where, $\phi(t)$ and $p(t) = \dot{\phi}(t)$ are the roll angle and the roll velocity, respectively, while $\varepsilon(t)$ represents the angle made by the keel mechanism with the axis of the center of gravity of the vessel as shown in Fig. 2, or in short, the keel angle. Here, $\tau_k(t)$ is the torque created by the moving keel, $\tau_d(t)$ is a disturbance torque created by time-varying load on the vessel and $\tau_{wi}(t)$ is the wave-induced disturbance torque. Regarding the constants, $I_x$ and $\Delta I_x$ denote the roll moment of inertia of the vessel and its hydrodynamic added mass coefficient, respectively. Linear and nonlinear positive drag coefficients of roll are $K_p$ and $K_{p|p|}$. The parameters $\rho$, $g$, $\nabla$, $\overline{GM}_m$ represent the density of water, gravity, the volume displacement of the vessel and the mean metacentric height, respectively, while $K_{\phi^3}$ accounts for the nonlinear part of the restoring forces.

The torque components mentioned in (1) collectively denote the overall torque acting on the vessel and can be represented as $\tau_{ol}$. Each of these torque components can be modelled as mentioned next.

*1) **Keel Torque** ($\tau_k$):* For the keel system, the torque $\tau_k$ comprises three components, represented as,

$$\tau_k = \tau_w - \tau_p - \tau_m \tag{2}$$

where, $\tau_w(t)$ is the torque due to the weight of the keel bulb, represented by,

$$\tau_w = -\left(m_k - \rho\nabla_k\right) g \left(z_k \sin\phi + L_k \sin(\varepsilon + \phi)\right) \tag{3}$$

And, $\tau_p(t)$ represents the torque arising out of the paddling effect of the keel, expressed as,

$$\tau_p = K_k(e+p) + K_{k|k|}(e+p)|e+p| + \Delta m_k(\dot{e}+\dot{p}) \tag{4}$$

Also, $\tau_m(t)$ which stands for the motor reaction torque can be expressed as,

$$\tau_m = J_{km}\dot{e} + B_{km}e = k_t I_a \tag{5}$$

In (3), the constants, $m_k$ and $\nabla_k$, denote the mass and the volume of the keel system, respectively. $z_k$ is the distance between the vessel's center of mass and the hinge point of

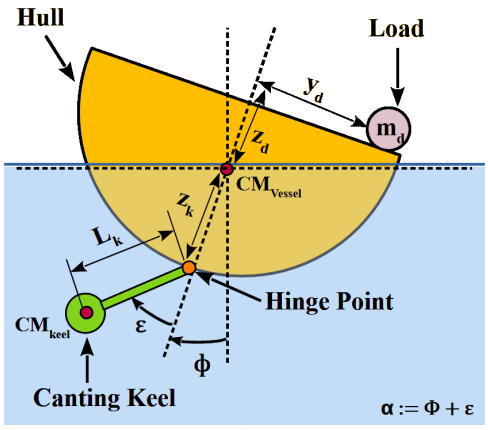


Fig. 2. Schematic of a typical monohull marine craft equipped with a canting keel mechanism [20]

the keel, whereas $L_k$ is the distance between the hinge point and mass/buoyancy center of the keel mechanism as depicted in Fig. 2. In (4), $e(t) = \dot{\varepsilon}(t)$ depicts the rate of change of the keel angle. $K_k$ and $K_{k|k|}$ represent the linear and nonlinear drag forces coefficients of the keel system, while $\Delta m_k$ is the added mass coefficient of the keel. In (5), $J_{km}$ is the motor inertia coefficient, $B_{km}$ is the motor damping coefficient, $k_t$ is the motor torque constant and $I_a$ is the armature current. The final form of the equations of the servo motor will be explained in Section II-B.

*2) **Load Torque** ($\tau_d$):* The effect of the load disturbance is introduced into the model via a torque in the vessel's frame whose lateral position varies with time. The disturbance torque $\tau_d(t)$ given in (1) can be represented in a similar manner to [21], as follows,

$$\tau_d = m_d g \left( z_d \sin\phi + y_d \cos\phi \right) \tag{6}$$

where $y_d(t)$ represents the time-varying lateral position of the load of mass $m_d$ in the vessel's frame as shown in Fig. 2, while $z_d(t)$ represents its vertical position from the center of mass of the vessel.

*3) **Wave-induced Torque** ($\tau_{wi}$):* The mathematical model for the wave-induced disturbances is typically based on the wave spectra and sea state parameters, which in turn influences the roll motion of the marine vessel. Although, one can imagine that the sea states are a complex amalgamation of sinusoidal waves of varying amplitudes and frequencies in space and time [3]. Therefore, in order to simplify this process, it is assumed that the sea states affecting the vessel can be approximated as a combination of N-sinusoidal waves, which gives rise to the wave-disturbance torque ($\tau_{wi}$). It can be represented in the form,

$$\tau_{wi} = \sum_{i=0}^{N} F_i \sin(\omega_i t) \tag{7}$$

where, $F_i$ and $\omega_i$ represent the amplitude and frequency of the $i^{th}$ torque component, respectively. The amplitudes ($F_i$) and frequencies ($\omega_i$) are chosen based on the FFT analysis of wave data gathered from field tests. For the simulation we have considered three wave components, i.e., $N = 3$. The data for the amplitudes ($F_i$) and frequencies ($\omega_i$) are provided later in Section V.

### B. Servo Motor Model

Assuming that the armature inductance ($L_a$) of the dc servo motor is negligible, the equations of the servo motor based on (5) can be expressed as,

$$\begin{cases} \tau_m = J_{km}\ddot{\varepsilon} + B_{km}\dot{\varepsilon} \\ \tau_m = k_t I_a \\ I_a = \frac{k_t}{R_a}(V_a - k_b\dot{\varepsilon}) \\ V_a = k_p(\varepsilon_d - \varepsilon) - k_d\dot{\varepsilon} \end{cases} \tag{8}$$

where, the symbols $J_{km}$, $B_{km}$, $k_t$ and $I_a$ denote the constants mentioned earlier. Also, $R_a$ stands for the armature resistance, $V_a$ denotes the armature voltage and $K_b$ represents the back-emf constant. Combining the equations in (8), leads to the final form of the servo motor equation, expressed as,

$$\ddot{\varepsilon} = \alpha_1\ \varepsilon + \alpha_2\ \dot{\varepsilon} + \beta_\varepsilon\ u \tag{9a}$$

where, the control signal $u$ is the desired keel angle, i.e. $u = \varepsilon_d$ and the other constants in (9a) can be written as,

$$\alpha_1 = \frac{-k_t^2 k_p}{J_{km} R_a}, \quad \beta_\varepsilon = \frac{k_t^2 k_p}{J_{km} R_a} \tag{9b}$$

$$\alpha_2 = \frac{-k_t^2(k_b + k_d) - R_a B_{km}}{J_{km} R_a} \tag{9c}$$

By combining (1) and (9a), the nonlinear form of roll-dynamics can be represented by the simplified notation,

$$\ddot{\phi} = f(\phi, \dot{\phi}, \varepsilon, \dot{\varepsilon}, \ddot{\varepsilon}) = f_\phi(\phi, \dot{\phi}, \varepsilon, \dot{\varepsilon}) + \beta_\phi u \tag{10a}$$

$$\beta_\phi = \frac{\beta_\varepsilon(\Delta m_k - J_{km})}{(I_x + \Delta I_x)} \tag{10b}$$

where the second part of the equation (10a) is written due to the fact that $\ddot{\varepsilon}$ is the only term that contains a linear function of $u$. It is to be noted here that gearbox ratio of 1:1 has been considered between the motor and the keel.

## III. Dynamic Properties of the System

Let the state vector be $\mathbf{x} = [\phi \quad \dot{\phi} \quad \varepsilon \quad \dot{\varepsilon}]$. The state equations can be written based on (10a) and (9a) as,

$$\begin{cases} \dot{x}_1 = x_2 \\ \dot{x}_2 = f_\phi(x_1, x_2, x_3, x_4) + \beta_\phi u + w \\ \dot{x}_3 = x_4 \\ \dot{x}_4 = \alpha_1\ x_3 + \alpha_2\ x_4 + \beta_\varepsilon\ u \\ y = x_1 \\ w = (\tau_d + \tau_{wi})/(I_x + \Delta I_x) \end{cases} \tag{11}$$

The system presented above is a $4^{th}$ order nonlinear system which is a combination of two subsystems: **1.** A second order nonlinear subsystem describing the dynamics of vessel and the torques affecting that. The input to this subsystem is the summation of different torques affecting the vessel and its states are $\phi$ and $\dot{\phi}$. **2.** A second order linear sub-system representing the servo motor and the keel system. The input to the linear subsystem is $\varepsilon_d$ (which is the input of the overall system as well) and its states are $\varepsilon$ and $\dot{\varepsilon}$. From (11), it is clear that relative degree of the system is two since the double derivative of the output $y$ is a function of the input $u$.

### A. Description of Torque Components

There is a strong interaction between the two subsystems mentioned above, as three of the torques applied to the vessel are determined by the linear subsystem. These three terms are $\tau_w$, $\tau_p$, and $\tau_m$, whose effect on the system will be explained in detail.

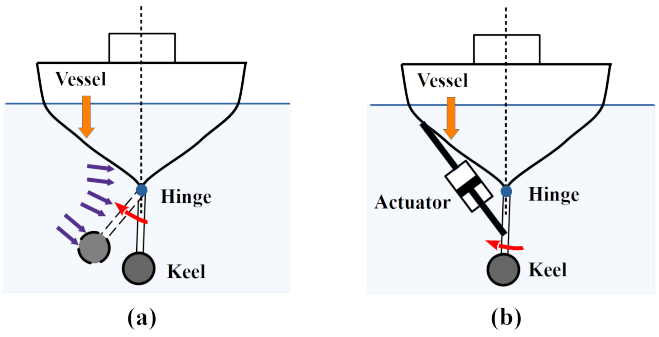


Fig. 3. Schematic representing the behaviour of (a) Paddling Torque ($\tau_p$) (b) Motor Reaction torque ($\tau_m$)

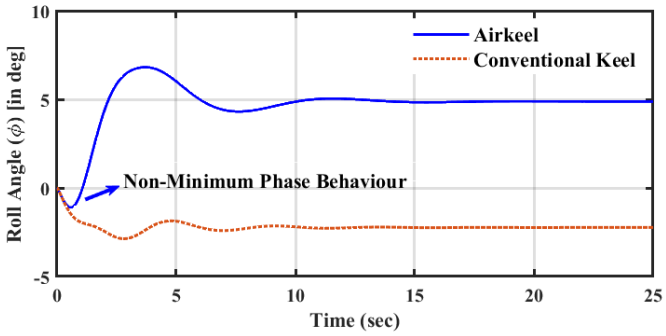


Fig. 4. Step responses of a typical marine vessel for the airkeel and the conventional keel

*1) Keel weight Torque ($\tau_w$):* This torque is only a function of keel and vessel positions, not their velocities or accelerations. This means that its dominant effect is on the steady-state position of the boat. It should also be noted that it represents both the airkeel (when $m_k < \rho\nabla_k$) and the conventional heavy keel (when $m_k > \rho\nabla_k$). According to (3), in the case of airkeel, an increment in $\varepsilon_d$ increases $\phi$, while it is the opposite for the conventional keel.

*2) Paddling Torque ($\tau_p$):* This torque arises due to the resistance exerted by the surrounding water on the movement of the keel and the connecting fin as shown in the illustration in Fig. 3 (a). As given in (4), the paddling torque is the summation of three components. The first two terms which represent the drag torque are proportional to the keel and boat velocities. In case of acceleration in the movement of keel and/or boat, the third term so called added mass torque is acting as well. Therefore, by increasing the keel angle as shown in Fig 3(a) a resistance torque is created in the water (blue arrows in the figure). Since the created torque acts on the hull of the boat (which is below the center of mass), it causes the roll angle to decrease. The opposite movement of the keel and boat due to the paddling effect is always the case regardless of the type of keel. The negative sign of $\tau_p$ in (2) represents this opposite movement.

*3) Motor Reaction Torque ($\tau_m$):* When the motor applies the torque $\tau_m$ to the keel, since the motor body is connected to the boat, an equal and opposite torque will be applied to the boat as well. Figure 3(b) visualizes this phenomenon, where the motor is replaced with a linear actuator for better intuition. As it is shown in the figure, if the goal is to increase the keel angle by retracting the actuator, it will decrease the roll angle simultaneously as the other end of actuator is connected to the boat. Similar to the paddling effect, this phenomenon is independent from the type of keel where the sign of $\tau_m$ in (2) is always negative.

### B. Effects on Roll Motion

In case of airkeel, the three torque components create a multi-directional effect on roll motion which results in opposite transient and permanent roll motions, unlike the conventional keel where they are unidirectional. The transient motion is due to $\tau_p$ and $\tau_m$ which oppose the keel direction, whereas the permanent position is created by $\tau_w$, which has similar direction as the keel. This behaviour is a well known phenomenon in control systems called *non-minimum phase* [17]. In terms of control, it is much more challenging to design a controller for the non-minimum phase airkeel compared to the minimum phase conventional keel. Therefore, we will specifically consider the airkeel for the upcoming sections.

In terms of the model in (1), the major difference between canting keel (CK) and the airkeel (AK) is the type of weight being put on the bulb, viz. positive for the CK and negative for the AK. This can be realised from (3) where the sign of term $m_k - \rho\nabla_k$ points either to AK ($\rho\nabla_k > m_k$) with buoyancy force pointing upwards or CK ($\rho\nabla_k < m_k$) with gravity force pointing downwards. To visualize the respective roll motions, the step responses of the nonlinear model of the both keels are plotted in Fig. 4. Moreover, the transfer functions representing the linearized model of both the canting keels are given as,

$$G_{CK}(s) = \frac{-0.90(s^2 + 0.04s + 3.35)}{(s^2 + 0.63s + 2.16)(s^2 + 1.88s + 6.26)} \quad (12)$$

$$G_{AK}(s) = \frac{-1.12(s + 1.52)(s - 2.48)}{(s^2 + 0.64s + 0.73)(s^2 + 2.33s + 11.73)} \quad (13)$$

where, $G_{CK}$ denotes the conventional keel and $G_{AK}$ represents the airkeel. It is evident from $G_{AK}$ that there exists an unstable zero in airkeel equipped vessels.

## IV. Control Design

### A. System Dynamics with Matched Disturbance

The roll dynamics model in (11) can be represented in a general form as,

$$\dot{\mathbf{x}} = f(\mathbf{x}) + \mathbf{b}u + w(\mathbf{x}) \quad (14)$$

$$y = x_1 \quad (15)$$

where, the disturbance $w(\mathbf{x})$ is bounded by a constant $W$ of known value, i.e.,

$$\|w(\mathbf{x})\| \leq W \quad (16)$$

The objective is to design a non-linear controller to achieve proper roll damping and disturbance rejection while maintaining the system stability. In order to do that, let us first assume, according to [17], that the disturbance ($w$) is matched and appears in the same channel as the input ($w_u$). Therefore, the redefined model can be written as below,

$$\dot{\mathbf{x}} = f(\mathbf{x}) + \mathbf{b}(u + w_u(\mathbf{x})) \tag{17}$$

**Remark:** Note that this is a strong assumption for the system under investigation since the disturbances are unmatched according to (14). However, we will later propose a modification to the control algorithm, which will be able to take care of the unmatched disturbances as well.

Now, by linearizing (17) around the equilibrium point, we have,

$$\dot{\mathbf{x}} = A\mathbf{x} + \mathbf{b}(u + w_u) + \Delta(\mathbf{x}) \tag{18}$$

where, $A$ is the Jacobian of $f(\mathbf{x})$ w.r.t $\mathbf{x}$ around the equilibrium point, $\mathbf{x}$ is the stater vector, $\mathbf{b}$ is the input matrix and $\Delta(\mathbf{x})$ stands for the higher order nonlinear terms and the the unmodelled dynamics of the system, which can be represented as,

$$\begin{aligned} \mathbf{x} &= [\phi \quad \dot{\phi} \quad \varepsilon \quad \dot{\varepsilon}]^T \\ \mathbf{b} &= [0 \quad \beta_\phi \quad 0 \quad \beta_\varepsilon]^T \\ \Delta(\mathbf{x}) &= [0 \quad \delta(\mathbf{x}) \quad 0 \quad \beta_\varepsilon]^T \end{aligned} \tag{19}$$

In order to segregate the *zero dynamics*, the system in (18), is written as two subsystems with the state vectors $\mathbf{z}_1$ and $\mathbf{z}_2$, where, $\mathbf{z}_2$ represents the zero dynamics [17].

*1)* ($\mathbf{z}_1$,$\mathbf{z}_2$)*-coordinate:* The order of the zero dynamics equation ($\mathbf{z}_2$) is equal to the relative degree ($r$) of the system, which is here equal to 2. Therefore, to find $\mathbf{z}_2$, $u$ should be eliminated from the last two state equations by a coordinate change. Assuming the new coordinate as $\mathbf{z} = [\mathbf{z}_1 \ \mathbf{z}_2]^T$, we have:

$$\mathbf{z} = \mathrm{T}\mathbf{x} \tag{20}$$

where, the transformation matrix T is chosen in a linear form since the state equations are linear in terms of $u$. In general T changes the last two states, but for our system $x_3$ remains a part of $\mathbf{z}_2$ since $\dot{x}_3$ does not include $u$ as shown in (11). In order to find the second element of $\mathbf{z}_2$, i.e., $z_{2,2}$, we have,

$$z_{2,2} = T_{41}x_1 + T_{42}x_2 + T_{43}x_3 + T_{44}x_4 \tag{21}$$

where, substitution of the state derivatives from (11) in the derivative form of (21) and equating the coefficient of $u$ to zero gives a possible solution as:

$$T_{41} = T_{43} = 0; \quad T_{42} = 1; \quad T_{44} = -\beta_\phi/\beta_\varepsilon \tag{22}$$

Now, the state equations in terms of $\mathbf{z}$ are as below:

$$\begin{bmatrix} \dot{\mathbf{z}}_1 \\ \dot{\mathbf{z}}_2 \end{bmatrix} = \begin{bmatrix} \mathbf{R} & \mathbf{S} \\ \mathbf{P} & \mathbf{Q} \end{bmatrix} \begin{bmatrix} \mathbf{z}_1 \\ \mathbf{z}_2 \end{bmatrix} + \begin{bmatrix} \mathbf{b}_1 \\ \mathbf{0} \end{bmatrix} (u + \bar{w}) + \begin{bmatrix} \boldsymbol{\delta}_1(\mathbf{z}_1, \mathbf{z}_2) \\ \boldsymbol{\delta}_2(\mathbf{z}_1, \mathbf{z}_2) \end{bmatrix} \tag{23}$$

where, $\mathbf{z}_1 = [\phi \ \dot{\phi}]^T$ and $\mathbf{z}_2 = [\varepsilon \ z_{2,2}]^T$. Also, $\mathbf{P}, \mathbf{Q}, \mathbf{R}$ and $\mathbf{S}$ are constant matrices of appropriate dimensions. Notice that $\bar{w}$ is eliminated from the second part of the state vector. As mentioned before, the second equation in (23), that is,

$$\dot{\mathbf{z}}_2 = \mathrm{P}\mathbf{z}_1 + \mathrm{Q}\mathbf{z}_2 + \boldsymbol{\delta}_2(\mathbf{z}_1, \mathbf{z}_2) \tag{24}$$

is referred to as the *zero-dynamics* of the system [17]. In case the zero dynamics is locally unstable, i.e., the matrix Q is not Hurwitz, the system is said to exhibit *non-minimum phase* (NMP) behaviour. For the system under investigation, one of the eigen values of the matrix Q is at $+2.48$, thus making it a *non-minimum phase* system. It is understandable from (24) that the stability of the zero dynamics should be taken care with the aid of $\mathbf{z}_1$, since the input does not affect $\mathbf{z}_2$ directly.

*2)* ($\sigma$,$\eta$)*-coordinate:* In order to design a sliding mode controller, a scalar sliding variable is considered in the following form,

$$\sigma = \dot{\phi} + \lambda\phi; \quad \lambda > 0 \tag{25}$$

Assuming $\sigma$ as the first state variable in the new coordinate, the rest of the state variables form the *internal dynamics* of the system, which can be defined as: $\boldsymbol{\eta} = [\phi \quad \epsilon \quad z_4]^T$. Notice that, $\boldsymbol{\eta}$ contains $\mathbf{z}_2$ and the lower derivatives of the output. Hence, it does not involve $u$ as well. Transforming (23) to the new coordinate, we have,

$$\begin{bmatrix} \dot{\sigma} \\ \dot{\boldsymbol{\eta}} \end{bmatrix} = \begin{bmatrix} \mathrm{R_m} & \mathbf{S_m} \\ \mathbf{P_m} & \mathbf{Q_m} \end{bmatrix} \begin{bmatrix} \sigma \\ \boldsymbol{\eta} \end{bmatrix} + \begin{bmatrix} \beta_\phi \\ \mathbf{0} \end{bmatrix} (u + w_u) + \begin{bmatrix} \boldsymbol{\delta}_\sigma(\sigma, \boldsymbol{\eta}) \\ \boldsymbol{\delta}_{\boldsymbol{\eta}}(\sigma, \boldsymbol{\eta}) \end{bmatrix} \tag{26}$$

where, $\mathbf{P_m}$, $\mathbf{Q_m}$, $\mathrm{R_m}$ and $\mathbf{S_m}$ are constant matrices of appropriate dimensions and can be found using the coordinate transformation. The idea is to bring the sliding variable $\sigma$ to zero (or a desired trajectory) in finite time using a sliding mode controller. Since the input has no direct effect on $\boldsymbol{\eta}$ and the $\boldsymbol{\eta}$-dynamics is unstable (notice that $Q_m$ is not Hurwitz as it includes the eigenvalues of $Q$), therefore, bringing $\sigma$ to zero does not stabilize the entire system. To handle this issue, the sliding variable can be modified [17], [18] as follows,

$$\sigma_m = \sigma - K\boldsymbol{\eta} \tag{27}$$

where, $K$ is a gain matrix of appropriate dimension.

*3)* ($\sigma_m$,$\eta$)*-coordinate:* Using (27), the new state space representation becomes,

$$\begin{bmatrix} \dot{\sigma}_m \\ \dot{\boldsymbol{\eta}} \end{bmatrix} = \begin{bmatrix} \mathrm{K}_\sigma & \mathbf{K}_{\boldsymbol{\eta}} \\ \mathbf{P_m} & \mathbf{P_m}K + \mathbf{Q_m} \end{bmatrix} \begin{bmatrix} \sigma_m \\ \boldsymbol{\eta} \end{bmatrix} + \begin{bmatrix} \beta_\phi \\ \mathbf{0} \end{bmatrix} (u + w_u) + \begin{bmatrix} \boldsymbol{\delta}_{\sigma_m}(\sigma_m + K\boldsymbol{\eta}, \boldsymbol{\eta}) \\ \boldsymbol{\delta}_{\boldsymbol{\eta}}(\sigma_m + K\boldsymbol{\eta}, \boldsymbol{\eta}) \end{bmatrix} \tag{28}$$

where,

$$\begin{aligned} \mathrm{K}_\sigma &= \mathrm{R_m} - K\mathbf{P_m} \\ \mathbf{K}_{\boldsymbol{\eta}} &= \mathrm{R_m}K + \mathbf{S_m} - K(\mathbf{P}_m K + \mathbf{Q}_m) \end{aligned} \tag{29}$$

As it can be seen from (28), the $\boldsymbol{\eta}$-equation contains a tuning parameter $K$, which can be utilized to place the eigen values of the matrix $(\mathbf{P}_m K + \mathbf{Q}_m)$ at desirable locations, assuming that the pair $(Q_m, P_m)$ is controllable. This, in turn, stabilizes the zero dynamics of the system. Now, in order to converge $\sigma_m$ to zero in finite time the following control law can be defined,

$$u = u_{eq} + u_s \tag{30a}$$

Here, $u_{eq}$ is chosen as follows to cancel the known terms of $\dot{\sigma}_m$ and to bring $\sigma_m$ to zero exponentially,

$$u_{eq} = -\frac{1}{b}[K_\sigma \sigma_m + \mathbf{K}_{\boldsymbol{\eta}} \boldsymbol{\eta} + \gamma \sigma_m] \tag{30b}$$

where, the gain $\gamma$ is a design parameter. Also, $u_s$ represents a switching controller which takes care of modelling uncertainties and finite-time convergence. It is defined as,

$$u_s = -\frac{1}{b}(\mu \ \text{sign}(\sigma_m)); \ \ \mu > 0 \tag{30c}$$

It can be noted from (28) that as $\sigma_m \rightarrow 0$, we can say that, $\boldsymbol{\eta} \rightarrow 0$, since the matrix $(\mathbf{P_m} K + \mathbf{Q_m})$ is Hurwitz, which further implies $\sigma \rightarrow 0$ based on (27). In other words, $[\sigma_m \quad \boldsymbol{\eta}]^T \rightarrow [\sigma_{md} \quad \boldsymbol{\eta}_d]^T$, which is equal to the $[0 \quad \mathbf{0}]^T$ in this case.

### B. System Dynamics with Unmatched Disturbances

The unmatched disturbances (which does not appear in the input channel), should be considered separately in our case, since the coordinate changes do not eliminate $w$, from the $\boldsymbol{\eta}$-dynamics. This means that $\eta_d$ is not zero anymore as it is affected by the disturbance as well. A practical example of such a unmatched disturbance event is when the boat deviates from the level position ($\phi = 0$) due to unbalanced loading scenarios on board the vessel. In order to bring the vessel back to the no-roll or zero-roll position, the keel needs to be at a certain non-zero angle ($\varepsilon_d \neq 0$) at steady state. Given that $\varepsilon$ is part of $\boldsymbol{\eta}$, this implies that $\boldsymbol{\eta}_d$ is non-zero as well. On the other hand to have $\sigma_d = 0$, from (27), $\sigma_m = -K\boldsymbol{\eta}_d$.

The control law in (26) does not fulfill the conditions in the case of unmatched disturbance, as in (26) $\sigma_m$ always goes to zero. To modify (26), a new sliding variable ($\tilde{\sigma}_m = \sigma_m - \sigma_{md}$) is defined. Based on this, the control law can be modified as,

$$\begin{aligned} u &= -\frac{1}{b}[K_\sigma \tilde{\sigma}_m + \mathbf{K}_{\boldsymbol{\eta}} \boldsymbol{\eta} + \gamma \tilde{\sigma}_m + \mu \ \text{sign}(\tilde{\sigma}_m)] \\ \tilde{\sigma}_m &= \sigma_m - K\boldsymbol{\eta}_d \end{aligned} \tag{31}$$

A practical choice is to consider $\boldsymbol{\eta}_d$ as time-invariant and equal to the desired steady state values of the state variables, which in our case is, $[0 \quad \varepsilon_d \quad 0]$. Now, to find $\varepsilon_d$ one can think $\varepsilon_d = -w_u^v$, where $w_u^v$ is a virtual matched disturbance which gives the same roll deviation as the effect of the unmatched disturbance. To estimate $w_u^v$, an extended state observer (ESO) can be designed as follows,

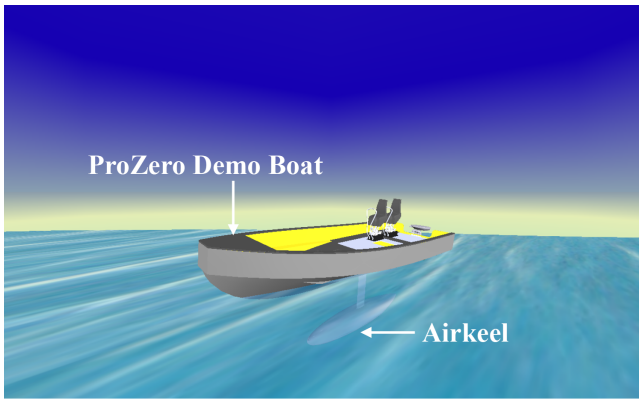


Fig. 5. Snapshot of the 3D animation of the Pro-Zero Demo boat for wave disturbance scenario in Simulink environment (Watch the video at this link: https://youtu.be/071SBK0P_oY)

$$\begin{aligned} \begin{bmatrix} \dot{\hat{\sigma}}_m \\ \dot{\hat{\boldsymbol{\eta}}} \\ \dot{\hat{w}}_u^v \end{bmatrix} &= \begin{bmatrix} \mathrm{K}_\sigma & \mathbf{K}_{\boldsymbol{\eta}} & \beta_\phi \\ \mathbf{P_m} & \mathbf{P_m} K + \mathbf{Q_m} & 0 \\ 0 & \mathbf{0} & 0 \end{bmatrix} \begin{bmatrix} \hat{\sigma}_m \\ \hat{\boldsymbol{\eta}} \\ \hat{w}_u^v \end{bmatrix} \\ &\quad + \begin{bmatrix} \beta_\phi & \mathbf{0} & 0 \end{bmatrix}^T u + L(y - \hat{y}) \end{aligned} \tag{32}$$

$$\hat{y} = \begin{bmatrix} 0 & I_\eta & 0 \end{bmatrix} \begin{bmatrix} \hat{\sigma}_m & \hat{\boldsymbol{\eta}} & \hat{w}_u^v \end{bmatrix}^T \tag{33}$$

where, $I_\eta = [1 \ 0 \ 0]$ and the observer gain ($L$) is designed through the steady-state kalman filter approach.

### C. Tuning the state feedback matrix

The $\eta$-dynamics subsystem shown in Fig. 4, can be rewritten as,

$$\begin{cases} \dot{\boldsymbol{\eta}} = \mathbf{Q_m} \boldsymbol{\eta} + \mathbf{P_m} \sigma + \boldsymbol{\delta}_\eta^{'}(\sigma, \boldsymbol{\eta}, w) \\ \sigma = K\boldsymbol{\eta} + \sigma_m \end{cases} \tag{34}$$

where, $\boldsymbol{\delta}_\eta^{'}(.)$ includes the nonlinear terms as well as the unmatched disturbances ($w$). In this subsystem, $K$ is a state feedback matrix where its main role is to stabilize the $\eta$-dynamics. Moreover, $K$ can be used to improve the performance and/or disturbance rejection. A proper solution to guarantee the stability while considering other objectives is the LQR control approach. Defining a cost function in the following form,

$$\min \ \mathbf{J} = \int_0^\infty \left( \boldsymbol{\eta}^T(t) Q_{\boldsymbol{\eta}} \boldsymbol{\eta}(t) + r_\sigma \sigma^2(t) \right) dt \tag{35}$$

where, $Q_{\boldsymbol{\eta}} = diag(q_\phi, q_\varepsilon, q_{z4})$, the solution would be in a state feedback form given in (34). To prioritize different objectives the weighting coefficients should be tuned properly.

## V. Simulation Studies

In this section, two case studies of a marine craft simulated on the MATLAB/Simulink environment are presented to demonstrate the effectiveness of our approach. In the first study, the roll damping capability is assessed for two

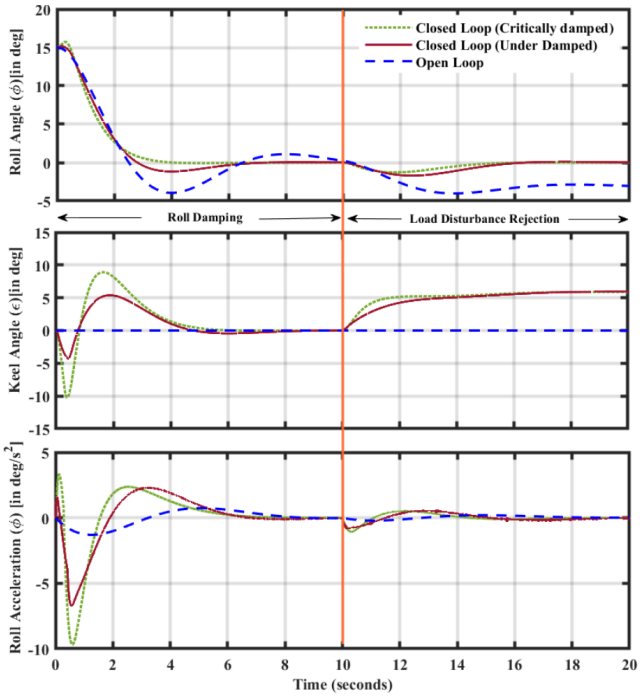


Fig. 6. Roll damping and load disturbance rejection in open loop and closed loop for an initial condition of $\phi = 15^\circ$ for the vessel and a sudden load of 300kgs introduced at 10 seconds.

different parametric combinations of the proposed control algorithm. Also, the vessel is subjected to a sudden load disturbance of 300kgs ($m_d$) midway during the simulation to exhibit the load disturbance rejection potential of the proposed approach. In the second study, the wave disturbance rejection capability of the proposed controller is evaluated for the same parametric combinations. This is done by introducing the wave-induced disturbance torque ($\tau_{wi}$) as described in Section II-A. These studies also provides insights on the effectiveness of the controller for seasickness reduction. The typical marine craft considered for these studies has an overall length ($L_{oa}$) of 14m and is fully-loaded at departure. This is simulated using the lumped parameter model as described in Section II. The necessary model parameters of the vessel, keel and servo motor are as $I_x = 125000$ kgm$^2$, $\Delta I_x = 31,250$ kgm$^2$, $\nabla = 20,000$ kg, $\overline{GM}_m = 1.06$ m, $K_p = 1\text{x}10^5$ kgm$^2$/s, $K_{p|p|} = 0.5\text{x}10^5$ kgm$^2$, $m_k = 150$ kg, $\nabla_k = 6$ m$^3$, $m_k = 150$ kg, $z_k = 1.4$ m, $L_k = 2.0$ m, $k_t = 100$ Nm/A, $k_b = 375$ Vs/rad, $R_a = 1\ \Omega$, $J_{km} = 20\text{x}10^3$ kgm$^2$ and $B_{km} = 100$ Nms/rad. The wave parameters are set as: $\omega_i = \{0.8; 1.0; 1.2\}$ rad/sec and $F_i = \{0.2\text{x}10^4, 1.2\text{x}10^4, 0.2\text{x}10^4\}$ Nm. From a practical point of view, a bound on the keel angle ($\varepsilon$) is set at $\pm 50^\circ$ for all cases. In order to visualize the dynamic behaviour of the system for the simulated cases, a 3D animation of the Pro-Zero demo boat (shown in Fig. 1) is made using the Simulink 3D Animation environment. A snapshot of the animation is shown in Fig. 5 and the corresponding video can be found at this link. For the purposes of this animation, only a single frequency has been chosen for the wave disturbances.

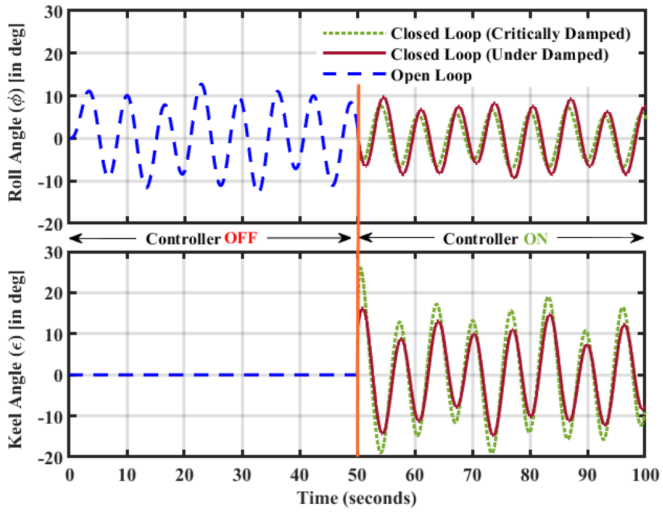


Fig. 7. Wave disturbance rejection in open loop and closed loop, considering the controller is activated after 50 seconds.

### A. Roll Damping and Load Disturbance Rejection

Fig. 6 shows $\phi$, $\varepsilon$ and roll acceleration ($\ddot{\phi}$) responses of the marine vessel under investigation. The responses are divided into two phases: the first phase of duration 0 - 10 seconds accounts for the roll damping scenario from an initial roll angle of 15°, whereas the second phase of duration 10 - 20 seconds exhibits the load disturbance scenario by applying 300 Kgs of load at the 10 sec mark. Both these scenarios are investigated for two distinct combinations of the controller parameters ($q_\phi, q_\varepsilon, q_{z4}$ and $r_\sigma$) which determine the gain matrix $K$ and the responses are compared with the open loop response of the system, which acts as the baseline for evaluating the performances.

In terms of roll damping, as the system is stable by nature, the rolling action of the vessel seems to settle down to a null position, even in open loop. However, as evident from Fig. 6, it takes a substantial amount of time (∼10 sec) and there is a significant undershoot. Fig. 6 shows also two possible closed loop responses designed by selecting different weighting coefficients in (35). The first controller is tuned to have a critically damped response (indicated in green) while the second one gives an under damped response (indicated in red). As it is clear from the $\ddot{\phi}$ profile that the critically damped response generates a higher acceleration, thus making it less feasible for sea sickness scenarios. However, for applications where faster roll damping is a priority such as cargo vessels, it would be a better solution. In the case of load disturbance rejection, Fig. 6 shows that the proposed algorithm in Section IV-B, successfully rejects the sudden load disturbance by changing the steady state value of $\varepsilon$. In terms of comparison, the critically damped response brings the vessel back to the null-roll condition faster, but at the cost of higher acceleration.

### B. Wave Disturbance Rejection

Fig. 7 shows the variation of $\phi$ and $\varepsilon$, when the system is subjected to wave disturbances as discussed in section

II-A. In the first 50 seconds, $\varepsilon$ is kept at zero (Controller is *off*), thereafter, the same controllers used in the roll damping scenario, are activated for the last 50 seconds. To evaluate the performance of these controllers against wave disturbances, the roll reduction percentage (RRP) metric is used, represented in [22] as,

$$RRP = \frac{R_{OL} - R_{CL}}{R_{OL}} \text{x} 100 \tag{36}$$

where, $R_{OL}$ stands for the rms value of the open loop roll response and $R_{CL}$ represents the rms value of the closed loop roll angle. The RRP values for the critically damped and under damped controllers are 38.17% and 22.63%, respectively. This indicates considerable improvement is achieved by the critically damped controller, as expected. The effect of the wave disturbances may be further reduced, by different selection of the controller parameters however this will cost in higher acceleration in roll damping and load disturbance rejection.

## VI. Concluding Remarks

This study focuses on the issue of roll stabilization of a marine vessel equipped with a canting keel mechanism, taking into account its dynamic properties such as the non-minimum phase behavior when the keel is positively buoyant. A nonlinear sliding mode control algorithm is designed such that it not only stabilizes the zero dynamics of the system, but it is also able to achieve acceptable roll damping and disturbance rejection of both matched and unmatched disturbances, such as those arising due to unbalanced loading and wave influence. The results of the simulation study on a considered vessel with typical features indicate that the choice of the control parameters, whether critically damped or under damped should depend on the modus operandi of the vessel, since a singular solution to all desirable features may be unreasonable.

## Acknowledgments

The authors would like to acknowledge the role of the AMCOSTAR Eurostars project for funding this project. We would also like to thank Dacoma ApS and Tuco Marine Group for sharing data regarding the vessel.

## References

[1] A. Koch, I. Cascorbi, M. Westhofen, M. Dafotakis, S. Klapa, and J. P. Kuhtz-Buschbeck, "The neurophysiology and treatment of motion sickness," *Deutsches Ärzteblatt International*, vol. 115, no. 41, p. 687, 2018.

[2] A. Wertheim, J. Bos, and W. Bles, "Contributions of roll and pitch to sea sickness," *Brain Research Bulletin*, vol. 47, no. 5, pp. 517–524, 1998.

[3] T. I. Fossen, *Handbook of marine craft hydrodynamics and motion control*. John Wiley & Sons, 2011.

[4] T. Perez, *Ship motion control: course keeping and roll stabilisation using rudder and fins*. Springer Science & Business Media, 2006.

[5] T. Perez and M. Blanke, "Ship roll damping control," *Annual Reviews in Control*, vol. 36, no. 1, pp. 129–147, 2012. [Online]. Available: https://www.sciencedirect.com/science/article/pii/S1367578812000119

[6] M. A. Irkal, S. Nallayarasu, and S. Bhattacharyya, "Cfd approach to roll damping of ship with bilge keel with experimental validation," *Applied Ocean Research*, vol. 55, pp. 1–17, 2016.

[7] A. F. Gawad, S. A. Ragab, A. H. Nayfeh, and D. T. Mook, "Roll stabilization by anti-roll passive tanks," *Ocean Engineering*, vol. 28, no. 5, pp. 457–469, 2001. [Online]. Available: https://www.sciencedirect.com/science/article/pii/S0029801800000159

[8] R. Moaleji and A. R. Greig, "On the development of ship anti-roll tanks," *Ocean Engineering*, vol. 34, no. 1, pp. 103–121, 2007. [Online]. Available: https://www.sciencedirect.com/science/article/pii/S0029801806000722

[9] L. Liang, Q. Cheng, and P. Cai, "Design of fin stabilizer controller during ship zig-zag motion," *Ocean Engineering*, vol. 252, p. 111049, 2022. [Online]. Available: https://www.sciencedirect.com/science/article/pii/S0029801822004668

[10] J. Gong, J. guo Liu, Y. xing Dai, C. yu Guo, and T. cheng Wu, "Dynamics of stabilizer fins on the waterjet-propelled ship," *Ocean Engineering*, vol. 222, p. 108595, 2021. [Online]. Available: https://www.sciencedirect.com/science/article/pii/S0029801821000305

[11] R. Li, T. Li, W. Bai, and X. Du, "An adaptive neural network approach for ship roll stabilization via fin control," *Neurocomputing*, vol. 173, pp. 953–957, 2016.

[12] W. Luo, B. Hu, and T. Li, "Neural network based fin control for ship roll stabilization with guaranteed robustness," *Neurocomputing*, vol. 230, pp. 210–218, 2017.

[13] N. C. Townsend and R. A. Shenoi, "Control strategies for marine gyrostabilizers," *IEEE Journal of Oceanic Engineering*, vol. 39, no. 2, pp. 243–255, 2013.

[14] L. Liang and Y. Wen, "Rudder roll stabilization with disturbance compensation model predictive control," *Journal of Marine Science and Technology*, vol. 24, no. 1, pp. 249–259, 2019.

[15] J. Zhao, C. Liang, and X. Zhang, "Rudder roll stabilization based on arc tangent nonlinear feedback for ships," *Journal of Marine Science and Engineering*, vol. 8, no. 4, p. 245, 2020.

[16] DACOMA. Airkeel. [Online]. Available: www.dacoma.dk/airkeel

[17] S. Gopalswamy and J. K. Hedrick, "Tracking nonlinear non-minimum phase systems using sliding control," *International Journal of Control*, vol. 57, no. 5, pp. 1141–1158, 1993.

[18] T. Lauvdal and T. I. Fossen, "Nonlinear rudder-roll damping of non-minimum phase ships using sliding mode control," in *1997 European Control Conference (ECC)*. IEEE, 1997, pp. 1689–1694.

[19] L. Xiao and J. Jouffroy, "Modeling and nonlinear heading control of sailing yachts," *IEEE Journal of Oceanic engineering*, vol. 39, no. 2, pp. 256–268, 2013.

[20] S. Chaudhuri, H. Ramezani, and J. Jouffroy, "Modelling and control of a canting keel-based ship roll stabilization system for crane operations," in *2022 IEEE International Conference on Systems, Man, and Cybernetics (SMC)*, 2022, pp. 1904–1909.

[21] J. He, L. Xiao, and J. Jouffroy, "Towards heading control of an autonomous sailing platform through weight balancing," *IFAC Proceedings Volumes*, vol. 45, no. 27, pp. 392–397, 2012, 9th IFAC Conference on Manoeuvring and Control of Marine Craft.

[22] X. Su, Y. Gao, and R. Zhao, "Roll attitude controller design for ships at zero speed," *International Journal of Fuzzy Systems*, vol. 20, no. 2, pp. 611–620, 2018.